Quantum-limited amplification with a nonlinear cavity detector

C. Laflamme and A. A. Clerk
Department of Physics, McGill University, Montreal, Quebec, Canada H3A 2T8
(Received 6 December 2010; published 7 March 2011)

We consider the quantum measurement properties of a driven cavity with a Kerr-type nonlinearity that is used to amplify a dispersively coupled input signal. Focusing on an operating regime that is near a bifurcation point, we derive simple asymptotic expressions describing the cavity's noise and response. We show that the cavity's backaction and imprecision noise allow for quantum-limited linear amplification and position detection only if one is able to utilize the sizable correlations between these quantities. This is possible when one amplifies a nonresonant signal but is not possible in quantum nondemolition qubit detection. We also consider the possibility of using the nonlinear cavity's backaction for cooling a mechanical mode.

DOI: 10.1103/PhysRevA.83.033803 PACS number(s): 42.60.Da, 03.65.Ta, 03.65.Yz

I. INTRODUCTION

A number of recent experiments has made use of driven microwave transmission-line resonators for sensitive near-quantum-limited measurements. These include measurements of the position of a nanomechanical oscillator near the standard quantum limit [1,2] as well as measurements of single and multiqubit systems in circuit QED setups [3,4]. Such experiments use the microwave cavity as an op-amp type amplifier [5], where the signal to be detected (e.g., the position x of a mechanical resonator or the σ_z operator of a qubit) is dispersively coupled to the microwave cavity, meaning that the cavity frequency depends on the signal. When the cavity is driven, the resulting modulation of the cavity frequency by the signal leads to a modulation of the phase of the reflected beam from the cavity. By monitoring this phase (e.g., via homodyne interferometry), one has essentially amplified the signal.

Most experiments using a cavity for such dispersive measurements and amplification have not exploited nonlinearities in the cavity—the cavity is just a driven damped harmonic oscillator. The resulting measurement and amplification properties of the system are well understood. In particular, it is known that this system can be used for quantum-limited linear amplification, meaning that the total added noise of the measurement can be as small as allowed by quantum mechanics (see, e.g., Ref. [5] for a pedagogical discussion).

While the linear-cavity regime is certainly useful, it is also interesting to consider another possibility afforded by microwave circuit cavities: They can be engineered to have strong Kerr-type nonlinearities through the use of Josephson junctions [6–8]. The resulting nonlinear cavity can then be used for amplification in ways not possible with a linear cavity. Attention has largely focused on using such devices in the scattering mode of operation, where the signal to be amplified is incident on the cavity from a coupled transmission line and where backaction effects are irrelevant. Experiments using this mode have realized single-quadrature amplification and squeezing [7,9–11]; this operation mode has also been the subject of many theoretical treatments, e.g., Refs. [6,7,12,13]. For qubit detection, another possibility is to use the bifurcation in a nonlinear cavity to give a latching-type measurement, where the final dynamical state of the cavity depends on the initial state of the qubit [14,15]; this scheme has also received theoretical attention [16].

Instead, in this paper, we will study theoretically the quantum measurement properties of a driven nonlinear cavity in the operation mode most relevant to experiments in nanomechanics and quantum information, the so-called op-amp mode of operation described above. Unlike the scattering mode studied in Refs. [6,7,12], here backaction is indeed relevant and plays a crucial role in enforcing the quantum limit on the added noise: To reach the quantum limit, the backaction noise must be as small as allowed by quantum mechanics [5,17]. We will focus exclusively on regimes where there is no multistability in the cavity dynamics (in contrast to the bifurcation amplifier setup). We note that experiments using a nonlinear microwave cavity amplifier in the op-amp mode discussed here have recently been performed. Hartridge *et al.* have constructed a nonlinear cavity formed by a superconducting quantum interference device (SQUID) [18] and have used this to detect a dispersively coupled superconducting qubit [19]. A recent experiment by Ong *et al.* [20] used a nonlinear microwave formed from a transmission line resonator and a Josephson junction to detect a dispersively coupled qubit; this experiment also investigated backaction effects.

Our analysis focuses on operation points close (but not past) the bifurcation in the cavity response, a regime that yields extremely large small-signal low-frequency amplification gain. The approach we use is standard: We linearize the cavity dynamics about its mean classical value and use the resulting linear quantum Langevin equations to study the noise properties of the cavity detector. This allows us to assess its ability to reach the op-amp amplifier quantum limit; a related analysis is presented in Ref. [8]. Despite this standard approach, we find a number of surprising conclusions that seem not to have been appreciated in the existing literature. In particular, we show that the nonlinear cavity near the bifurcation is equivalent to a degenerate parametric amplifier (DPA) driven with a *detuned pump* [21]. The value of this effective detuning is not an independent parameter and tends to a universal value as one approaches the bifurcation. This mapping allows us to derive simple analytic asymptotic expressions for the cavity's noise and gain that are universally valid as one approaches the bifurcation point.

In the low-frequency limit, large-gain limit, we find that the imprecision noise of the cavity is precisely four times what would be expected of an ideal resonantly pumped degenerate parametric amplifier with equivalent gain [cf. Eqs. (45) and (46)]. We also show, somewhat surprisingly, that the cavity's backaction noise at low frequencies is always given by the same simple expression valid for a linear cavity, an expression that is usually interpreted as describing the overlap of displaced coherent states [cf. Eqs. (49) and (50)]. We find that the nonlinear cavity amplifier is quantum limited at low frequencies but *only* if one can make use of the large correlations between the backaction and imprecision noises. Such correlations cannot be utilized simply in quantum nondemolition (QND) qubit detection; hence, the cavity amplifier misses the quantum limit on QND qubit detection by a large factor.

We also use our approach to study the possibility of using the backaction of a nonlinear-driven microwave cavity to cool a nanomechanical resonator. Near the bifurcation point, we find an extremely simple expression for the effective temperature of the nonlinear cavity's backaction [cf. Eq. (60)]; surprisingly, the only relevant cavity parameter is its damping rate κ. We also show that a driven nonlinear cavity is far better at cooling a low-frequency mechanical oscillator than a corresponding driven linear cavity with comparable parameters. This latter conclusion matches what was found by Nation *et al.* [8], who studied backaction cooling by a nonlinear cavity numerically over a wide range of cavity parameters, including regimes where there is bistability in the cavity dynamics. Aspects of cooling and heating using a driven nonlinear cavity were also addressed by Dykman [22].

The remainder of this paper is organized as follows. In Sec. II, we review the basics of how one uses a nonlinear cavity as a linear op-amp style amplifier and review the formulation and origin of the quantum limit applicable here. In Sec. III, we show how, near the bifurcation, the nonlinear cavity is equivalent to a DPA driven by a detuned pump. In Sec. IV, we use this mapping to derive asymptotic expressions for the cavity's noise and amplifier gain near the bifurcation point and assess its ability to reach the quantum limit for small signal frequencies. Section V extends this analysis to nonzero signal frequencies. Finally, in Sec. VI, we consider the asymmetric quantum backaction noise of the cavity and assess the possibility of using the cavity for backaction cooling a mechanical oscillator.

II. BASICS OF A NONLINEAR CAVITY AMPLIFIER

A. System Hamiltonian

The Hamiltonian of a cavity detector with a Kerr-type nonlinearity has the general form

$$\hat{H} = \hat{H}_{\rm sys} + \hat{H}_\kappa = \hbar\omega_c \hat{a}^\dagger \hat{a} - \hbar\Lambda \hat{a}^\dagger \hat{a}^\dagger \hat{a}\hat{a} + \hat{H}_\kappa, \qquad (1)$$

where ω_c is the cavity resonance frequency and Λ is the Kerr constant. We take $\Lambda > 0$ in what follows, as is appropriate for a microwave cavity incorporating Josephson junctions; the results are easily generalized to $\Lambda < 0$. The term $\hat{H}_\kappa$ represents the damping (at rate κ) and driving of the cavity due to its coupling to extra cavity modes (e.g., in a microwave circuit, to the transmission line used to drive the cavity). Derivations of this Hamiltonian for microwave circuits incorporating Josephson junctions are presented in many places in the literature, and we do not repeat them here (see, e.g., Refs. [6–8,12,18]); a schematic is presented in Fig. 1. In writing Eq. (1), we have assumed the relevant case of a high-Q cavity and, thus, made use of the rotating wave approximation to write the nonlinear term. We will also be interested throughout in the case of a weak nonlinearity, $\Lambda \ll \kappa$. For clarity, we focus exclusively on the ideal case where there is no internal cavity loss; we also focus on the case of a one-sided cavity. Our analysis could be easily generalized to incorporate either a two-sided cavity or internal loss (see, e.g., Ref. [12]).

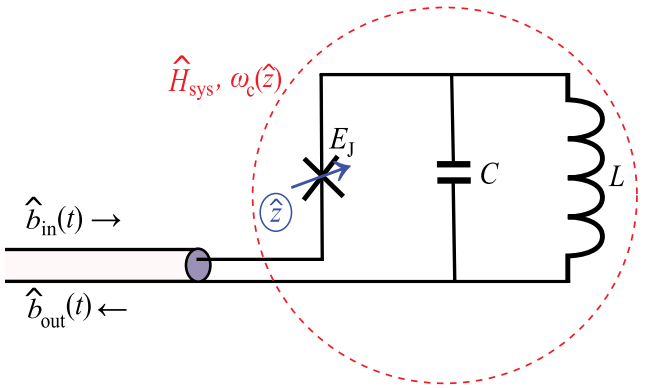

FIG. 1. (Color online) Schematic of a realization of the nonlinear cavity amplifier. The cavity is formed by an LC circuit containing a Josephson junction (energy E_J). The cavity is damped and is driven by a coupled transmission line; $\hat{b}_{\rm in}$ and $\hat{b}_{\rm out}$ denote the input and output fields in the transmission. The input signal $\hat{z}$ is a flux that controls the value of E_J and, hence, the frequency of the cavity ω_c. An experimental realization of this system is presented in Ref. [18].

Unlike a linear cavity, the nonlinear cavity described by Eq. (1) can undergo a bifurcation as a function of its parameters from a regime where the average cavity photon number $\bar{n} = \langle \hat{a}^\dagger \hat{a} \rangle$ is a single-valued function of the drive frequency ω_d, to a regime where it is multivalued. For drive strengths just below the bifurcation threshold, $\bar{n}$ is a single-valued function of drive frequency but exhibits a very pronounced slope (see Fig. 2). This extreme sensitivity to cavity frequency makes the cavity an extremely sensitive dispersive detector and amplifier in this regime. However, it is not *a priori* obvious whether the cavity's noise in this regime is small enough to allow quantum-limited performance. Answering this question is our main goal.

B. Quantum limit on amplification in the op-amp mode of operation

We focus throughout on the op-amp mode of amplifier operation, where the input signal to be detected (described by an operator $\hat{z}$) is coupled directly to the cavity photon number:

$$H_{\rm int} = A\hat{a}^\dagger \hat{a}\hat{z} \equiv \hat{F}\hat{z}. \qquad (2)$$

The operator $\hat{z}$ could represent (for example) the position of a nanomechanical beam (as considered in Ref. [8]) or the signal flux applied to a SQUID circuit (as in Ref. [18]). As a result of this dispersive coupling, the cavity frequency and

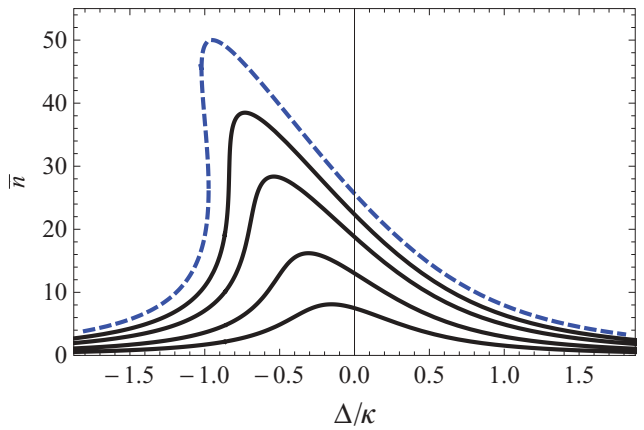

FIG. 2. (Color online) Average cavity photon number $\bar{n}$ versus drive detuning $\Delta = \omega_d - \omega_c$ for various driving strengths $\bar{b}_{\rm in}$. The curves show the evolution of the cavity response as one goes through the bifurcation: Solid curves are for $\bar{b}_{\rm in} < \bar{b}_{\rm in,bif}$, while the dashed curve is for $\bar{b}_{\rm in} > \bar{b}_{\rm in,bif}$. The diverging slope of $d\bar{n}/d\Delta$ near the bifurcation allows for amplification with a large gain.

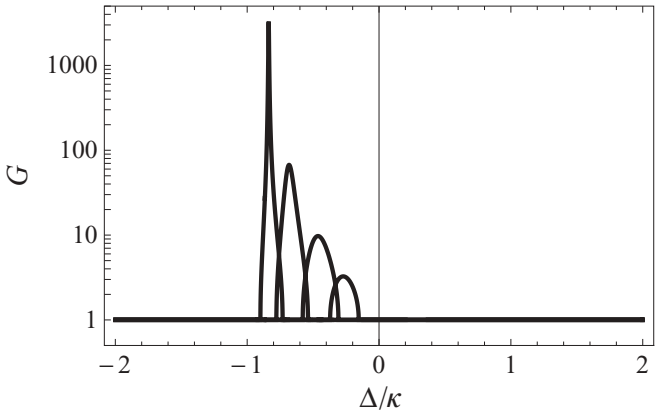

FIG. 3. Parametric zero-frequency photon number gain $G \equiv G[0]$ versus drive detuning Δ for various driving strengths $\bar{b}_{\rm in} < \bar{b}_{\rm in,bif}$ (same values as in Fig. 2). The gain is maximized near values of the detuning where the slope $d\bar{n}/d\Delta$ is maximal.

reflected-beam phase shift become z dependent; thus, one can amplify $z(t)$ by monitoring this phase. We will focus here on homodyne detection, where the output beam is interfered with a classical reference beam, and the resulting intensity is measured using a square-law detector. Letting $\hat{b}_{\rm out}(t)$ denote the output field from the cavity (as defined in standard input-output theory [23,24]), the measured homodyne intensity will be described by an operator $\hat{I}(t)$,

$$\hat{I} = B\sqrt{\kappa/2}[e^{i\phi}\hat{b}_{\rm out}(t) + \text{ H.c.}], \tag{3}$$

where ϕ is the phase of the classical reference beam and B is a dimensionless constant proportional to the amplitude of this beam. Note that $\hat{I}$ has units corresponding to a photon flux. As the value of B plays no role in what follows (it is just a scale factor for the output), we set $B = 1$ without loss of generality in what follows.

We will be interested in weak enough couplings that our cavity acts as a linear amplifier. As such, we have a linear relation between the input signal and the cavity output,

$$\langle\hat{I}(t)\rangle = \int_{-\infty}^{\infty} dt' \chi_{IF}(t-t')\langle\hat{z}(t')\rangle, \tag{4}$$

where $\chi_{IF}(t) \propto A$ is the forward gain of the amplifier and is determined by a standard Kubo formula [5].

The amplifier output (i.e., I) will have fluctuations even in the absence of any coupling to the detector; these are described by the symmetrized spectral density:

$$\bar{S}_{II}[\omega] = \frac{1}{2}\int_{-\infty}^{\infty} dt\ e^{i\omega t}\langle\{\hat{I}(t),\hat{I}(0)\}\rangle. \tag{5}$$

Again, as we are interested in linear amplification, the expectation value is taken in with respect to the state of the *uncoupled* detector (i.e., $A = 0$). It is useful and standard to think of these intrinsic output fluctuations in terms of effective signal (i.e., z) fluctuations; thus, we introduce the imprecision noise spectral density:

$$\bar{S}_{zz}[\omega] = \bar{S}_{II}[\omega]/|\chi_{IF}[\omega]|^2. \tag{6}$$

In the op-amp mode of operation, a second crucial aspect of the amplifier's noise is its backaction. By virtue of the the detector-signal coupling in Eq. (2), the operator $\hat{F} = A\hat{a}^\dagger\hat{a}$ (i.e., the cavity photon number) acts as a noisy backaction force on the signal. Extra fluctuations in $\hat{z}$ due to this stochastic force will necessarily increase the noise in the output of the amplifier and, thus, are part of the total added noise of the amplifier. The backaction force noise is characterized by a symmetrized noise spectral density $\bar{S}_{FF}[\omega]$ defined analogously as Eq. (5).

Thus, we have that the total amplifier contribution to the output noise has contributions from both imprecision and backaction noises. It is convenient (and common) to think of this total added noise in terms of a noise temperature $T_N[\omega]$: The total amplifier added noise at frequency ω is equivalent to the extra equilibrium noise we would get by raising the temperature of the signal source by $T_N[\omega]$.[1] This quantity is relevant no matter what the signal, be it the position of a harmonic oscillator or the voltage produced by some input circuit; we also stress that achieving the quantum limit on the noise temperature is equivalent to achieving the quantum limit on continuous weak displacement detection [5].

Minimizing the noise temperature at a given frequency requires one to first optimize the signal source's susceptibility $\chi_{zz}[\omega]$. This linear-response susceptibility tells us how the average value of $\hat{z}$ changes in response to a perturbation that couples to $\hat{z}$, i.e.,

$$\delta\langle\hat{z}(t)\rangle = \int_{-\infty}^{\infty} dt' \chi_{zz}(t-t')\langle\hat{F}(t')\rangle. \tag{7}$$

[1]We use the standard convention in which the noise temperature $T_N[\omega]$ is defined by assuming the signal source is initially at a temperature much larger than $\hbar\omega$. This definition leads to the standard bound given in Eq. (12).

Optimizing the total added noise over the coupling strength and phase of the signal source's susceptibility $\chi_{zz}[\omega]$ yields a standard bound on $T_N[\omega]$ [5],

$$\frac{k_B T_N[\omega]}{\hbar\omega} \geqslant \frac{1}{\hbar}\left\{\sqrt{\bar{S}_{zz}[\omega]\bar{S}_{FF}[\omega] - [\mathrm{Re}(\bar{S}_{zF}[\omega])]^2} - \mathrm{Im}\bar{S}_{zF}[\omega]\right\}, \tag{8}$$

where the inequality becomes an equality for an optimal source susceptibility satisfying

$$|\chi_{zz}[\omega]| = \sqrt{\bar{S}_{zz}[\omega]/\bar{S}_{FF}[\omega]}, \tag{9a}$$

$$\frac{\mathrm{Re}\ \chi_{zz}[\omega]}{|\chi_{zz}[\omega]|} = \frac{\mathrm{Re}\ \bar{S}_{zF}[\omega]}{\sqrt{\bar{S}_{zz}[\omega]\bar{S}_{FF}[\omega]}}. \tag{9b}$$

We have introduced the correlator $\bar{S}_{zF}$, which describes possible correlations between backaction and imprecision noises:

$$\bar{S}_{zF}[\omega] = \frac{\bar{S}_{IF}[\omega]}{\chi_{IF}[\omega]} = \frac{\int_{-\infty}^{\infty} dt e^{i\omega t}\langle\{\hat{I}(t),\hat{F}(0)\}\rangle}{2\chi_{IF}[\omega]}. \tag{10}$$

Consider the simple case where the signal frequency ω is much smaller than the relevant frequency scales of the cavity; thus, we may focus on the noise temperature in the $\omega \to 0$ limit. Using the fact that there cannot be any out-of-phase noise correlations at zero frequency (i.e., $\bar{S}_{zF}[0] = \mathrm{Re}\ \bar{S}_{zF}[0]$), the zero-frequency form of the fundamental Heisenberg inequality on detector noise [5],

$$\bar{S}_{zz}[0]\bar{S}_{FF}[0] - (\bar{S}_{zF}[0])^2 \geqslant \hbar^2/4 \tag{11}$$

implies that

$$k_B T_N \geqslant \hbar\omega/2, \tag{12}$$

i.e., the added noise amplifier must at least be as large as the zero-point noise of the signal source [5,17].[2] We stress that, while the conclusion may appear similar, the op-amp quantum limit considered here is *not* identical to the quantum limit on the scattering mode described in the seminal works by Haus and Mullen [25] and Caves [26]: the scattering-mode quantum limit does not involve backaction. Moreover, an amplifier may reach the quantum limit in the scattering mode but not in the op-amp mode [5].

The case where the input signal $\hat{z}$ is the spin operator of a qubit is also interesting. Here, the quantum limit on QND qubit detection involves the measurement rate Γ_{meas} and the measurement-induced backaction dephasing rate Γ_φ [27,28],

$$\Gamma_\varphi \geqslant \Gamma_{\mathrm{meas}}, \tag{13}$$

where for weak coupling:

$$\Gamma_\varphi = 2\bar{S}_{FF}[0]/\hbar^2, \tag{14a}$$

$$\Gamma_{\mathrm{meas}} = (2\bar{S}_{zz}[0])^{-1}. \tag{14b}$$

Thus, reaching the quantum limit on QND qubit detection places more stringent requirements on the detector than those required to have a quantum-limited noise temperature: Not only must the quantum noise bound of Eq. (11) be satisfied as an equality, but also there must be no backaction-imprecision correlations (e.g., $\bar{S}_{zF}[0] = 0$).

In Secs. III– VI, we will calculate the nonlinear cavity's noise and response functions and determine whether they reach the quantum limit on their noise temperature and on QND detection. We note in passing that Ref. [8] also addresses the quantum limit on amplification (specifically position detection) using a nonlinear cavity in a similar regime to that considered here. Their analysis is based on alternative formulation of the quantum limit, which is not equivalent to the one discussed here; in particular, they did not address whether the nonlinear cavity optimizes the quantum noise inequality of Eq. (11) or consider its noise temperature as defined in Eq. (8).

III. BEHAVIOR NEAR BIFURCATION

A. Mapping to a degenerate parametric amplifier

We begin our analysis by using standard input-output theory [23,24] to derive the Heisenberg equation of motion for the cavity field, in the absence of any coupling to the signal:

$$\frac{d}{dt}\hat{a} = -\frac{i}{\hbar}[\hat{a}, H_{\mathrm{sys}}] - \frac{\kappa}{2}\hat{a} - \sqrt{\kappa}\hat{b}_{\mathrm{in}}(t). \tag{15}$$

Here, $\hat{b}_{\mathrm{in}}(t) = \bar{b}_{\mathrm{in}}e^{-i\omega_d t} + \hat{\xi}(t)$ describes the input field incident on the cavity from the transmission line; its average value $\bar{b}_{\mathrm{in}}$ describes the coherent drive applied to the cavity at frequency $\omega_d = \omega_c + \Delta$, while $\hat{\xi}(t)$ describes quantum and classical noises entering the cavity from the drive port. Without loss of generality, we take the drive amplitude $\bar{b}_{\mathrm{in}}$ to be real and positive.

We are interested in driving strengths that result in a large average number of quanta $\bar{n}$ in the cavity but at the same time, are not so strong that there is multistability in the classical cavity dynamics. Thus, it is useful to write the cavity annihilation operator $\hat{a}$ as the sum of a classical and quantum part: This takes the form

$$\hat{a}(t) = e^{-i\omega_d t}e^{i\phi_a}(\sqrt{\bar{n}} + e^{i\pi/4}\hat{d}(t)). \tag{16}$$

The complex number $e^{i\phi_a}\sqrt{\bar{n}} \equiv \langle\hat{a}\rangle$ is simply determined by the classical equations of motion, whereas, $\hat{d}$ describes the influence of noise (and eventually, the coupling to the input signal). We have chosen the phase of the second term in Eq. (16) to simplify the following analysis. From Eq. (15), we find that the average cavity photon number $\sqrt{\bar{n}}$ is determined by the classical equation,

$$\bar{n}[(\kappa/2)^2 + (2\Lambda\bar{n} + \Delta)^2] = \kappa(\bar{b}_{\mathrm{in}})^2. \tag{17}$$

We can now use Eq. (15) to write an equation for $\hat{d}$; retaining only leading terms in $\bar{n} \gg 1$ yields a linear equation,

$$\frac{d}{dt}\hat{d} = -\frac{i}{\hbar}[\hat{d}, H_{\mathrm{dpa}}] - \frac{\kappa}{2}\hat{d} - \sqrt{\kappa}\hat{\xi}(t), \tag{18}$$

[2]Note that we have used the form of the quantum noise inequality corresponding to a vanishing reverse gain, i.e., coupling to $\hat{I}$ cannot change the average value of $\hat{F}$. The vanishing of the reverse gain for our nonlinear cavity amplifier is explicitly demonstrated in the Appendix.

where

$$\hat{H}_{\rm dpa} = -\hbar\widetilde{\Delta}\hat{d}^\dagger\hat{d} + i\hbar\frac{\tilde{g}}{2}(\hat{d}^\dagger\hat{d}^\dagger - \hat{d}\hat{d}). \tag{19}$$

Equation (19) is simply the Hamiltonian of a DPA driven by a nonresonant pump, where a single pump mode photon can be converted into two signal mode photons and vice versa (see, e.g., Ref. [24]). Here, the classical cavity field $\bar{a}$ plays the role of the pump mode, while the displaced cavity field $\hat{d}$ plays the role of the signal mode. The effective parametric interaction strength $\tilde{g}$ and effective pump detuning $\widetilde{\Delta}$ are given by

$$\tilde{g} = 2\Lambda\bar{n}, \tag{20a}$$

$$\widetilde{\Delta} = \Delta + 4\Lambda\bar{n}. \tag{20b}$$

The above mapping of the driven nonlinear cavity to a detuned DPA is general and only relies on $\bar{n} \gg 1$. We will be especially interested in operating points near the point of bifurcation, as these allow a maximal amplifier gain. As one approaches the bifurcation, the effective DPA parameters $\tilde{g}, \widetilde{\Delta}$ approach universal values. To see this, note first that a standard analysis of the classical equations of motion shows that the bifurcation occurs at a critical drive amplitude $\bar{b}_{\rm in,bif}$ satisfying

$$[\bar{b}_{\rm in,bif}]^2 = \frac{1}{6\sqrt{3}}\frac{\kappa^2}{\Lambda}. \tag{21}$$

For $\bar{b}_{\rm in} < \bar{b}_{\rm in,bif}$, $\bar{n}$ is a single-valued function of Δ. For $\bar{b}_{\rm in} = \bar{b}_{\rm in,bif}$, the slope of $\bar{n}$ versus Δ is infinite at a single point $\Delta = \Delta_{\rm bif}$; one finds from Eq. (17),

$$\Delta_{\rm bif} = -\frac{\sqrt{3}}{2}\kappa, \tag{22a}$$

$$\bar{n}_{\rm bif} = \frac{1}{2\sqrt{3}}\frac{\kappa}{\Lambda}. \tag{22b}$$

Thus, it follows from Eqs. (20) that the parameters of the effective DPA attain universal values at the bifurcation:

$$\tilde{g}_{\rm bif} = \frac{\kappa}{\sqrt{3}}, \tag{23a}$$

$$\widetilde{\Delta}_{\rm bif} = \frac{\kappa}{2\sqrt{3}}. \tag{23b}$$

Note crucially that, for cavity operating points near the bifurcation, *the effective DPA pump detuning $\widetilde{\Delta}$ is nonzero*. As we will see in Sec. III B, this will have a pronounced impact: *The amplified and squeezed quadratures of the DPA are not orthogonal*. This, in turn, has a significant effect on the noise properties of the nonlinear cavity detector.

B. Amplified cavity quadrature

To appreciate the implications of pump detuning in our effective paramp model, we consider the equations of motion corresponding to Eq. (19). We will be interested throughout in parameter regimes where this effective paramp has a photon number gain larger than 1; this necessarily requires $\tilde{g} > |\widetilde{\Delta}|$. In such regimes, the analysis is most conveniently presented by first introducing canonically conjugate quadrature operators $\hat{X}$ and $\hat{P}$,

$$\hat{X} = \frac{1}{\sqrt{2}}(e^{-i\theta/2}\hat{d} + e^{i\theta/2}\hat{d}^\dagger), \tag{24a}$$

$$\hat{P} = \frac{-i}{\sqrt{2}}(e^{-i\theta/2}\hat{d} - e^{i\theta/2}\hat{d}^\dagger), \tag{24b}$$

where the angle θ ($-\pi/2 \leqslant \theta \leqslant \pi/2$) is given by

$$\sin\theta = \widetilde{\Delta}/\tilde{g}. \tag{25}$$

As we will see, the above definition ensures that $\hat{X}$ is the quadrature amplified by the cavity. We also define corresponding quadratures $\hat{X}_{\rm in}$ and $\hat{P}_{\rm in}$ of the operator $\hat{\xi}$ associated with noise entering the drive port [e.g., these are defined by substituting $\hat{d} \to \hat{\xi}$ in Eqs. (24)].

With these definitions, the equations of motion are easily solved upon Fourier transforming (see Appendix),

$$\hat{X}[\omega] = -\sqrt{\kappa}\{\chi_1[\omega]\hat{X}_{\rm in}[\omega] - \tan\theta(\chi_1[\omega] - \chi_2[\omega])\hat{P}_{\rm in}[\omega]\}, \tag{26a}$$

$$\hat{P}[\omega] = -\sqrt{\kappa}\chi_2[\omega]\hat{P}_{\rm in}[\omega], \tag{26b}$$

where the susceptibilities χ_1, χ_2 are given by

$$\chi_1[\omega] = (-i\omega + \kappa/2 - \sqrt{\tilde{g}^2 - \widetilde{\Delta}^2})^{-1}, \tag{27a}$$

$$\chi_2[\omega] = (-i\omega + \kappa/2 + \sqrt{\tilde{g}^2 - \widetilde{\Delta}^2})^{-1}. \tag{27b}$$

For the case of a resonant pump (i.e., $\widetilde{\Delta} = \theta = 0$), these equations take a simple form and describe the usual behavior of a DPA: As $\tilde{g}$ approaches $\kappa/2$ from below (the parametric threshold), $\kappa\chi_1[0] \to \infty$, $\kappa\chi_2[0] \to 1$, and $\hat{X}$ ($\hat{P}$) is the amplified (squeezed) quadrature. By considering quadratures of the output field leaving the cavity, one finds that the photon number gain for the X quadrature is given by

$$G[\omega] \equiv |1 - \kappa\chi_1[\omega]|^2. \tag{28}$$

We will refer to $G[\omega]$ as the parametric gain of our system in what follows. For a resonant pump, the amplified and squeezed quadratures are clearly orthogonal (i.e., canonically conjugate). Note that $G[\omega]$ has a Lorentzian form, implying that there is only appreciable gain for frequency in a bandwidth Ω_B,

$$\Omega_B \equiv 1/\chi_1[0]. \tag{29}$$

We refer to Ω_B as the parametric bandwidth in what follows; in the large parametric gain limit, $\Omega_B \sim \kappa/\sqrt{G[0]}$.

The situation is more involved in the case of interest here, where the effective pump is not resonant [cf. Eqs. (23b)], and, hence, $\theta \neq 0$. We still have a parametric threshold when $\tilde{g}$ approaches $\sqrt{\kappa^2/4 + \widetilde{\Delta}^2}$ from below; as before, $\kappa\chi_1[0] \to \infty$ in this limit, while $\kappa\chi_2[0] \to 1$. It is easy to verify from Eqs. (23) that the parametric threshold coincides with the cavity bifurcation. It also follows from Eqs. (26) that, for any pump detuning $\widetilde{\Delta}$, $\hat{X}$ is the amplified quadrature: noise (or signal) incident in the X quadrature (i.e., $\hat{X}_{\rm in}$) *only* drives the X cavity quadrature and is multiplied by the large susceptibility χ_1. The photon number gain for signals in the X quadrature continues to be described by Eq. (28); as expected, this gain diverges as one approaches the bifurcation (see Fig. 3). As one

approaches the bifurcation, Eqs. (23) imply that the angle θ, which defines $\hat{X}$, takes the universal value:

$$\theta_{\rm bif} = \pi/6. \tag{30}$$

More troublesome, when $\widetilde{\Delta} \neq 0$, are the dynamics of the P quadrature, the quadrature orthogonal to the amplified quadrature. For a nonzero detuning, P is *not* the squeezed quadrature. Noise or signals incident on the cavity in the P quadrature (i.e., $\hat{P}_{\rm in}$) appear both in the cavity P quadrature (where it is multiplied by the small susceptibility χ_2), *as well* as in the cavity X quadrature, where it is also amplified (i.e., multiplied by the large susceptibility χ_1).

To summarize, we have shown that, near the bifurcation, the driven nonlinear cavity of Eq. (1) maps onto a DPA with a nonzero pump detuning $\widetilde{\Delta}$. This nonzero detuning means that the dynamics does not correspond to the simple situation of canonically conjugate amplified and squeezed quadratures. As we will see, this lack of orthogonality will have pronounced implications on the cavity noise properties near the bifurcation.

C. Coupling to signal and cavity gain

To complete our mapping of the nonlinear cavity detector to a DPA, we need to restore the signal-detector coupling Hamiltonian and consider the forward gain $\chi_{IF}(t)$ of the system [cf. Eq. (4)]. This forward gain tells us how strongly the input signal $\hat{z}$ influences the output homodyne current and will *not* be identical to the parametric photon number gain G discussed above. While one could calculate $\chi_{IF}[\omega]$ directly using a Kubo formula, it is simpler here to simply rederive the equations of motion for the cavity field including the coupling to $\hat{z}$. Retaining only leading-order terms in $\bar{n}$, the signal-cavity coupling Hamiltonian $H_{\rm int}$ in Eq. (2) retains the form $\hat{H}_{\rm int} = \hat{F}\hat{z}$, with the generalized force operator $\hat{F}$ taking the form:

$$\hat{F} \equiv A\hat{a}^\dagger\hat{a} \simeq (\sqrt{2\bar{n}}A)(\sin\nu\hat{X} + \cos\nu\hat{P}), \tag{31}$$

where

$$\nu \equiv \theta/2 + 3\pi/4. \tag{32}$$

We have dropped a constant term in $\hat{F}$, which can be absorbed into the Hamiltonian of the signal source. We see that, in general, the input signal $\hat{z}$ couples to both $\hat{X}$ and $\hat{P}$ and, thus, will enter the linearized cavity equations of motion as a driving term for both these quadratures. To be explicit, one should make the following replacements in Eqs. (26):

$$\hat{X}_{\rm in}[\omega] \to \hat{X}_{\rm in}[\omega] - \left(\sqrt{\frac{2\bar{n}}{\kappa}}A\cos\nu\right)\hat{z}[\omega], \tag{33a}$$

$$\hat{P}_{\rm in}[\omega] \to \hat{P}_{\rm in}[\omega] + \left(\sqrt{\frac{2\bar{n}}{\kappa}}A\sin\nu\right)\hat{z}[\omega]. \tag{33b}$$

Note that, at the bifurcation, the angle ν takes on the universal value:

$$\nu_{\rm bif} = \pi/12 + 3\pi/4 = 5\pi/6 = \pi - \theta_{\rm bif}. \tag{34}$$

Having characterized the signal-detector coupling, we now turn to the output homodyne current [cf. Eq. (3)]. This current is essentially one quadrature of the cavity output field and may be written

$$\hat{I}[\omega] = \sqrt{\kappa}(\cos\varphi_h\hat{X}_{\rm out}[\omega] + \sin\varphi_h\hat{P}_{\rm out}[\omega]), \tag{35}$$

where φ_h is determined by the phase of the reference beam used in the homodyne measurement and the output operators are given by the standard input-output relations [23,24], e.g.,

$$\hat{X}_{\rm out}[\omega] = \hat{X}_{\rm in}[\omega] + \sqrt{\kappa}\hat{X}[\omega]. \tag{36}$$

Thus, it follows from Eqs. (26) and (33) that the linear-response gain of the cavity amplifier will have the general form

$$\chi_{IF}[\omega] = \hbar A\sqrt{2\bar{n}}\kappa(\lambda_1\chi_1[\omega] + \lambda_2\chi_2[\omega]), \tag{37}$$

where

$$\lambda_1 = \cos\varphi_h(\cos\nu + \tan\theta\sin\nu), \tag{38a}$$

$$\lambda_2 = -\sin\nu(\cos\varphi_h\tan\theta + \sin\varphi_h). \tag{38b}$$

IV. AMPLIFIER NOISE IN THE LARGE GAIN LOW-FREQUENCY LIMIT

We are most interested in the properties of our cavity amplifier close to the bifurcation, where the parametric gain defined in Eq. (28) satisfies $G[0] \equiv G \gg 1$. In this regime, we expect amplification of input signals in a narrow band of frequencies $\omega < \Omega_B \sim \kappa/\sqrt{G}$. Thus, we begin our analysis by considering the amplifier noise to leading order in the large parameter G and for $\omega \ll \Omega_B$; the latter condition allows us to take the zero-frequency limit of cavity noise and response functions. We also assume the ideal case where the cavity is only driven by vacuum noise. Note that it is straightforward to use Eq. (17) to determine how G behaves as a function of driving strength as one approaches the bifurcation from below. Assuming that the drive detuning Δ is always chosen in order to maximize G, one finds that, near the bifurcation,

$$G \sim 4\left(\frac{|\bar{b}_{\rm in,bif}|^2}{|\bar{b}_{\rm in,bif}|^2 - |\bar{b}_{\rm in}|^2}\right)^3. \tag{39}$$

We start with the amplifier's forward gain. In the limit, $G \to \infty$. Equation (37) yields

$$\chi_{IF}[0] \sim \sqrt{2\bar{n}\kappa}A\lambda_1\sqrt{G}. \tag{40}$$

As expected, the forward gain is (to leading order) proportional to the square root of the DPA photon number gain.

Turning to the cavity output noise, we note that, for $G \gg 1$ and for small frequencies, Eqs. (26) yields that the cavity $\hat{P}$ quadrature is negligible in comparison to the $\hat{X}$ quadrature. As such, we can drop the second term in Eq. (35) and treat the homodyne current operator $\hat{I}$ as being proportional to $\hat{X}_{\rm out} \propto \hat{X} \propto \sqrt{G}$, Thus, for $G \to \infty$,

$$\hat{I}[\omega] \sim \kappa\cos\varphi_h\hat{X}[\omega]. \tag{41}$$

Looking at Eq. (31) for the backaction force operator $\hat{F}$, we see a similar argument holds. Thus, to leading order in G, $\hat{F}$ is also proportional to $\hat{X} \propto \sqrt{G}$:

$$\hat{F}[\omega] \sim \sqrt{2\bar{n}}A\sin\nu\hat{X}[\omega]. \tag{42}$$

Thus, to leading order in G, *backaction and imprecision noises are perfectly correlated with one another*, as they only differ by a constant. Their spectral densities will simply be proportional to the spectral density of the amplified cavity quadrature $\hat{X}$.

A. Imprecision noise

The leading-order-in-G intrinsic output noise of the amplifier (i.e., noise in the homodyne current at $A = 0$), thus, follows easily from Eqs. (41) and (26a) (see the Appendix). In the low-frequency limit, we have

$$\bar{S}_{II}[0] \sim \frac{\kappa}{2}\cos^2\varphi_h G(1+\tan^2\theta). \tag{43}$$

The two terms in the last factor represent two distinct physical contributions to the output noise. The θ-independent term arises from X-quadrature input noise ($\hat{X}_{\rm in}$) being amplified and appearing in $\hat{X}$. In contrast, the term proportional to $\tan^2\theta$ is a direct consequence of the nonzero effective pump detuning $\widetilde{\Delta}$. The resulting nonorthogonality of amplified and squeezed quadratures causes P-quadrature input noise ($\hat{P}_{\rm in}$) *also* to be amplified and to appear in the amplifier output $\hat{I}$. Thus, we see that $\widetilde{\Delta} \neq 0$ causes the output noise to be larger than what would be expected for a resonant pump DPA with equivalent photon number gain G.

Combing the above expression with Eq. (40) for the gain, we find that the low-frequency imprecision noise [cf. Eq. (6)] near the bifurcation (i.e., $G \to \infty$) is given by

$$\bar{S}_{zz}[0] \sim \bar{S}_{zz,\rm ideal}[0] h_{\rm imp}(\theta,\nu), \tag{44}$$

where

$$\bar{S}_{zz,\rm ideal} = \left(\frac{\hbar^2\kappa}{4\bar{n}A^2}\right), \tag{45a}$$

$$h_{\rm imp}(\theta,\nu) = \frac{1+\tan^2\theta}{(\cos\nu+\sin\nu\tan\theta)^2}. \tag{45b}$$

Here, $\bar{S}_{zz,\rm ideal}$ is the imprecision noise of an ideal DPA in the large gain limit. By ideal, we mean a DPA that was pumped on resonance, and where the input signal z only drives the amplified X quadrature [i.e., the angle ν in Eq. (31) would be zero]. $h_{\rm imp}(\theta,\nu) > 1$ describes the increase of $\bar{S}_{zz}$ due to the fact that our nonlinear cavity does not realize a DPA in this ideal fashion. The numerator of $h_{\rm imp}$ describes the extra output noise due to the nonresonant effective pump as discussed after Eq. (43). The denominator describes the reduction in gain coming from the fact that the signal drives both the $\hat{X}$ and the $\hat{P}$ quadratures.

Finally, we can further simplify our result by using the fact that, near the point of bifurcation, the effective DPA parameters approach universal values [cf. Eq. (23)]. For leading order, we can simply replace θ by its value at the bifurcation $\theta_{\rm bif} = \pi/6$. Thus, we obtain our final expression for the imprecision near the bifurcation:

$$\bar{S}_{zz}[0] \sim 4\bar{S}_{zz,\rm ideal}. \tag{46}$$

In the large gain limit, the imprecision of the nonlinear cavity amplifier is a factor of 4 times what would be expected from a theoretically ideal degenerate parametric amplifier. The behavior of the imprecision noise relative to the ideal value is shown in Fig. 4.

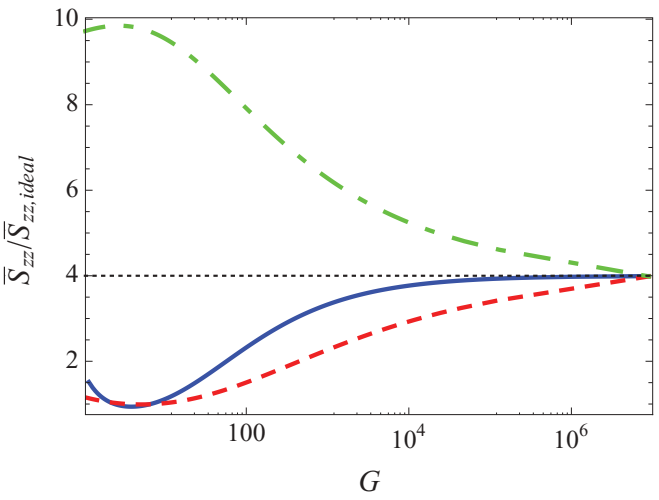

FIG. 4. (Color online) Imprecision noise $S_{zz}[0]$, scaled by the imprecision noise of an ideal DPA, $\bar{S}_{zz,\rm ideal}$ versus parametric photon number gain G. For large G, the imprecision noise is four times the ideal value. (Solid blue) Increase G by increasing the drive amplitude $\bar{b}_{\rm in}$ toward $\bar{b}_{\rm in,bif}$, using an optimal Δ for each drive strength. (Dashed red) Fix $(\bar{b}_{\rm in}/\bar{b}_{\rm in,bif})^2 = 0.995$; increase G by tuning Δ to approach the optimal value from below. (Long dash-short dash, green) Same as previous, but increase G by tuning Δ to approach the optimal value from above.

B. Backaction noise and backaction-imprecision product

From Eq. (42), we see that to leading order in G, the low-frequency backaction noise spectral density $\bar{S}_{FF}[0]$ will just be proportional to the low-frequency output noise spectral density $\bar{S}_{II}[0]$. Using the universality of the DPA parameters near the bifurcation, we find that, in the $G \to \infty$ limit,

$$S_{FF}[0] \sim \frac{1}{3}\frac{A^2\bar{n}}{\kappa}G. \tag{47}$$

We see the backaction diverges as the parametric photon number gain G; this is a simple consequence of the fact that our dispersive coupling unavoidably leads the signal $\hat{z}$ to be coupled to the amplified cavity quadrature X. The full expression (valid for arbitrary G) is not too unwieldy and is given in the Appendix as Eq. (A14). Note that similar spectral densities for a nonlinear cavity were calculated using a linearized Fokker-Planck approach in Refs. [16] and (in the classical high-temperature regime) [29].

Combining our results, we see that, near the bifurcation, the backaction-imprecision product will be much larger than the minimum value of $\hbar^2/4$ allowed by quantum mechanics. In the large-G limit, we have

$$\bar{S}_{FF}[0]\bar{S}_{zz}[0] \sim \frac{G}{3}\hbar^2. \tag{48}$$

Figure 5 shows the scaling of $\bar{S}_{FF}[0]\bar{S}_{zz}[0]$ versus parametric gain G as one approaches the bifurcation by either tuning the drive detuning Δ or tuning the drive strength $\bar{b}_{\rm in}$; the universal asymptotic behavior described by Eq. (48) is clear.

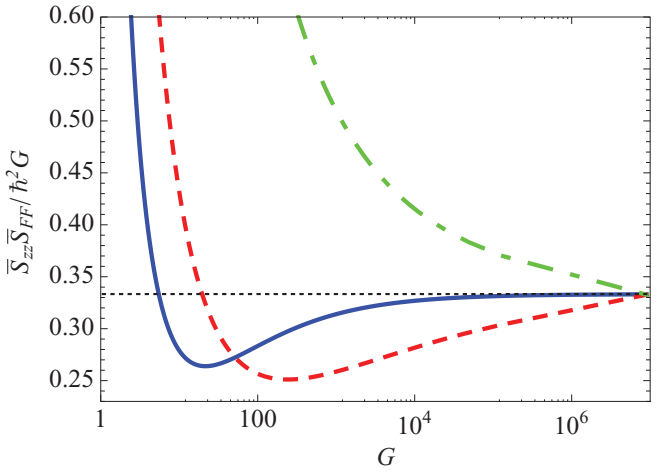

FIG. 5. (Color online) Backaction-imprecision product $\bar{S}_{zz}[0]\bar{S}_{FF}[0]$ (scaled by $\hbar^2 G$) versus parametric photon number gain G, demonstrating the universal scaling predicted for large G. Individual curves correspond to the same parameters as in Fig. 4.

The above result implies that, if one cannot make use of backaction-imprecision noise correlations, one is very far from having a quantum-limited device. In particular, *near the bifurcation, the nonlinear cavity detector cannot be used for QND qubit detection*: In such an experiment, the backaction dephasing rate will be a factor $G \gg 1$ larger than the minimum rate dictated by quantum mechanics [cf. Eq. (13)]. Note that the situation is very different for a linear cavity: there, as long as one drives the cavity on resonance, the $\bar{S}_{FF}[0]\bar{S}_{zz}[0]$ product attains the minimum possible value of $\hbar^2/4$ [5,30].

It is tempting to think that, by simply changing the cavity operating point slightly, one could achieve a situation where the input signal is only coupled to the cavity quadrature $\hat{P}$ and, thus, avoid the problematic diverging backaction found above. From Eqs. (31) and (32), we see that this would require an operating point for which the angle $\theta = \pi/2$. However, from Eqs. (25) and (27), this, in turn, implies that the cavity would have no parametric gain: $G = 1$. Thus, one cannot solve the problem of large backaction by simply changing the drive detuning without simultaneously getting rid of the amplifier gain.

C. Comparison with linear-cavity backaction formula

For a linear cavity, one can directly connect the backaction noise spectral density at zero frequency to how strongly the average cavity amplitude $\langle \hat{a} \rangle$ changes in response to a change in the signal. One finds

$$\bar{S}_{FF,\mathrm{lin}}[0] = A^2 \left| \frac{d\langle \hat{a} \rangle}{d\Delta} \right|^2. \tag{49}$$

This elegant result was first derived in Ref. [31] in the case where $\hat{z}$ is a spin operator for a qubit; $\bar{S}_{FF}[0]$, in this case, is directly proportional to the qubit dephasing rate [cf. Eq. (14a)]. Heuristically, it expresses the fact that the backaction disturbance of the measurement is directly related to the distinguishability of cavity states associated with different values of the input signal. A small change in the input signal causes a small displacement of the coherent state describing the cavity. Equation (49) implies that the backaction dephasing Γ_φ (and, hence, $\bar{S}_{FF}$) is directly determined by the overlap between this displaced coherent state and the original coherent state describing the cavity.

One would not expect Eq. (49) to apply, in general, to our nonlinear cavity detector, as now the intracavity state corresponding to a given fixed value of the input signal is *not* a coherent state or even a pure state [32]. This is a direct result of the squeezing and amplification of the cavity noise that occurs as one approaches the bifurcation. However, if one is far from the bifurcation, these effects should be minimal, and one might expect Eq. (49) to remain valid. This idea was put forward recently in Ref. [20] and was derived within an approximation that neglects noise squeezing of the cavity. Our approach fully accounts for the squeezing of the intracavity fluctuations and allows us to test the general validity of Eq. (49). Surprisingly, we find that this expression *exactly* captures the full backaction noise, even close to the bifurcation:

$$\bar{S}_{FF,\mathrm{lin}}[0] = \bar{S}_{FF}[0]. \tag{50}$$

Here, $\bar{S}_{FF}[0]$ is the full expression for the backaction noise spectral density that follows from Eqs. (26) [see Eq. (A14)]. We see that, despite the fact that the cavity is not in a coherent state or even a pure state, Eq. (49) remains valid for the nonlinear cavity amplifier; that this should be so is by no means *a priori* obvious.

Reference [20] also suggests that the nonlinear cavity detector reaches the quantum limit on QND detection [cf. Eq. (13)], implying that the backaction-imprecision product $\bar{S}_{FF}\bar{S}_{zz}$ attains its minimum possible value of $\hbar^2/4$. In contrast, we find that the backaction noise $\bar{S}_{FF}$ (and, hence, backaction dephasing rate) is a factor $G \gg 1$ larger than the quantum-limited value [cf. Eq. (48) and Fig. 5]. Here, the discrepancy arises from the fact that Ref. [20] does not explicitly calculate the measurement rate (i.e., $1/\bar{S}_{zz}$) for a specific optimized cavity readout scheme but rather assumes that it also be given (up to a prefactor) by overlap expression in Eq. (49). This would imply the measurement imprecision noise $\bar{S}_{zz}[0]$ scales like $1/G$ in the large-G limit. In contrast, we explicitly consider homodyne detection of the cavity output. We find that the imprecision noise (and, hence, measurement rate) are independent of G in the large gain limit, in agreement with Ref. [18]. This is a simple consequence of the fact that the nonlinear cavity's parametric gain amplifies both the signal *and* the vacuum fluctuations driving it by the same factor of $\sqrt{G}$.

D. Quantum limit on the amplifier added noise

While in the low-frequency large gain limit, the nonlinear cavity system cannot function as a quantum-limited QND qubit detector; nonetheless, it may be a quantum-limited linear amplifier (i.e., have the minimum noise temperature T_N allowed by quantum mechanics). This difference stems from the fact that, when used as an amplifier (in the op-amp mode), one can take advantage of correlations between backaction and imprecision noises by tuning the susceptibility of the signal source (e.g., in a voltage amplifier, the source impedance).

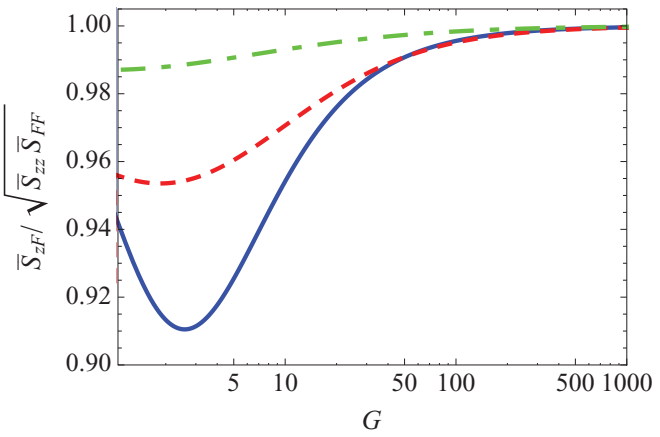

FIG. 6. (Color online) Backaction-imprecision correlations as measured by $\bar{S}_{zzF}[0]/\sqrt{\bar{S}_{zz}[0]\bar{S}_{FF}[0]}$ versus parametric photon number gain G. As expected, the curves all tend to the universal value of 1 as $G \to \infty$. Individual curves correspond to the same parameters as in Fig. 4.

To leading order in G and at low frequencies, we have shown that the backaction and output noise operators are proportional to one another, implying perfect correlation:

$$\bar{S}_{zF}[0] \sim \sqrt{\bar{S}_{zz}[0]\bar{S}_{FF}[0]}. \tag{51}$$

Figure 6 shows the behavior of these correlations versus G, where G is tuned is various ways; the asymptotic perfect correlation behavior is clear.

Turning to Eq. (8) for the optimized noise temperature T_N, we see that perfectly correlated backaction and imprecision noises do not contribute. This implies that our leading-order-in-G analysis is insufficient to determine whether T_N is quantum limited: This analysis only tells us that there is no order-$\sqrt{G}$ term in T_N. To determine whether the quantum limit is reached near the bifurcation, one must go beyond leading-order expressions, although we are interested in the low-frequency limit. Such an analysis is straightforward, although tedious; details are presented in the Appendix. Obtaining the cavity noise correlators and forward gain exactly from Eqs. (26) with no large-G assumption, we find that, at zero frequency, *the nonlinear cavity detector always optimizes the quantum noise inequality of Eq.* (11) *(i.e., it is satisfied as an equality)*. As such, the minimal low-frequency noise temperature given by Eq. (8) is indeed the quantum-limited value of $\hbar\omega/2$. We stress that this result is completely independent of the choice of homodyne phase φ_h.

E. Utility of backaction-imprecision correlations

As always, achieving a quantum-limited noise temperature is not simply a question of having an amplifier that saturates the fundamental quantum noise inequality of Eq. (11)—one also needs to optimally tune the susceptibility $\chi_{zz}[\omega]$ of the signal source (i.e., the source impedance). This optimization results in two conditions, cf. Eqs. (9). The magnitude condition [cf. Eq. (9a)] can always be achieved by an appropriate tuning of the signal-detector coupling A; it corresponds to properly balancing the relative contributions of backaction and imprecision noises to the total added noise. In contrast, the phase condition [cf. Eq. (9b)] cannot be achieved by simply tuning A. It corresponds to optimizing $\chi_{zz}[\omega]$ to optimally make use of in-phase backaction-imprecision correlations described by $\mathrm{Re}\bar{S}_{zF}$.

Consider the nonlinear cavity detector in the low-frequency large gain regime considered above. We found that it has a maximal value of correlations $\bar{S}_{zF}$, Eq. (51). Equation (9b) then implies that reaching the quantum limit on the noise temperature requires $\mathrm{Im}\chi_{zz}[\omega] = 0$. This is in sharp contrast to the more common situation where $\bar{S}_{zF}$ vanishes, and the optimal source susceptibility χ_{zz} must be purely imaginary.

This has interesting consequences. For concreteness, consider the case where our input system is a mechanical oscillator and z represents a position $\chi_{zz}[\omega]$ is simply given by

$$\chi_{zz}[\omega] = \frac{-1/m}{\omega^2 - \omega_M^2 + i\omega\gamma}. \tag{52}$$

Here, ω_M is the resonance frequency of the mechanical oscillator, m is its mass, and γ is its damping rate. We see that $\chi_{zz}[\omega]$ is purely real if one is far from resonance, i.e., $|\omega - \omega_M| \gg \gamma$. Thus, the nonlinear cavity detector is ideally suited to applications where one is interested in nonresonant position detection. For example, standard interferometric gravitational wave detectors require sensitive position detection of a test mass in the free-mass limit, i.e., $\omega_M \to 0$ [33]. In this case, as long as $\omega \gg \gamma$, one always has a nonresonant situation, and χ_{zz} is real. For such frequencies, the nonlinear cavity amplifier would be able to achieve a quantum-limited noise temperature. In contrast, if one used a detector with $\bar{S}_{zF} = 0$ in this regime, the noise temperature is, at best, a factor $\omega_M/\gamma \gg 1$ larger than the quantum-limited value. The utility of using correlations between backaction and imprecision noises is well known in the gravitational wave community [34], although it is not usually discussed in terms of the general noise temperature language used here.

Finally, we note that, if the input signal $\hat{z}$ was a voltage and we think of our cavity amplifier as a voltage amplifier, the requirement that the input susceptibility be purely real to optimize the noise temperature translates into requiring a signal source with a purely imaginary source impedance [5].

V. AMPLIFIER NOISE AT NONZERO FREQUENCIES

It is straightforward to extend our analysis to describe the amplification of signals with frequencies ω that are nonzero but still small enough that the parametric gain $G[\omega] \gg 1$. It follows from Eq. (28) that, in the $G[0] \gg 1$ limit, this requires $\omega \leqslant \Omega_B \sim \kappa/\sqrt{G[0]}$. Simple analytic expressions are easily obtained in the limit where $G[0] \to \infty$ while ω/Ω_B stays finite. For leading order in $G[0]$, one finds (as expected) that the photon number gain $G[\omega]$ and forward gain $\chi_{IF}[\omega]$ have a Lorentzian frequency dependence on a scale set by Ω_B. Letting $\tilde{\omega} = \omega/\Omega_B$, we have

$$G[\omega] = \frac{G[0]}{1+\tilde{\omega}^2}, \tag{53a}$$

$$\chi_{IF}[\omega] = \frac{\chi_{IF}[0]}{1 - i\tilde{\omega}}. \tag{53b}$$

In the same limit, we find that the imprecision noise is frequency independent, whereas, the remaining correlators

also decay with frequency on a scale set by Ω_B:

$$\bar{S}_{zz}[\omega] = \bar{S}_{zz}[0], \tag{54a}$$

$$\bar{S}_{FF}[\omega] = \frac{\bar{S}_{FF}[0]}{1+\tilde{\omega}^2}, \tag{54b}$$

$$\bar{S}_{zF}[\omega] = \frac{\bar{S}_{zF}[0]}{1+i\tilde{\omega}}. \tag{54c}$$

It immediately follows that, for finite frequencies, the noise temperature behaves as

$$k_B T_N[\omega] \simeq \hbar\omega\left[\sqrt{\frac{1}{4}+\frac{G}{3}\left(\frac{\tilde{\omega}}{1+\tilde{\omega}^2}\right)^2}+\sqrt{\frac{G}{3}}\frac{\tilde{\omega}}{1+\tilde{\omega}^2}\right]. \tag{55}$$

Thus, we see that, at finite frequencies, the reduced noise temperature $2k_B T_N/\hbar\omega$ rapidly increases as a function of frequency from the quantum-limited value of 1; in particular, it is already much greater than 1 for frequencies small enough to not appreciably reduce the gain. The leading correction at finite ω comes from the imaginary part of the noise cross correlator $\bar{S}_{zF}[\omega]$. As discussed extensively in Ref. [5], such out-of-phase backaction-imprecision correlations cannot be taken advantage of by simply tuning the susceptibility of the source; as a result, their existence represents unused information and, thus, leads to a departure from the quantum limit. In principle, such correlations can be utilized via feedback techniques.

VI. BACKACTION COOLING

In the preceding analysis, we have seen that, near the bifurcation point, the backaction noise of the nonlinear cavity amplifier diverges; this prevents quantum-limited amplification unless one can make use of noise correlations. In this section, we change focus somewhat and consider the specific case where the input signal $\hat{z}$ is the position of a mechanical resonator. In this case, the large backaction of the nonlinear cavity may actually be useful: It has the potential to strongly cool the mechanical resonator toward its quantum ground state.

The topic of backaction cooling has received considerable attention in the optomechanics and electromechanics communities [35]. It has been shown that the backaction of a *linear* cavity dispersively coupled to a mechanical resonator can be used to ground-state cool the mechanical resonator if one is in the so-called good cavity limit, where the mechanical frequency ω_M is much larger than the cavity damping rate κ [36,37]. This regime has been exploited in recent experiments with linear microwave cavities [38,39] and optical cavities [40–42].

In the opposite regime of a low-frequency mechanical resonator ($\omega_M \ll \kappa$), cooling using a linear cavity is still possible, but the lowest achievable temperature is on the order of $T_{\rm BA} \sim \kappa/k_B$. A crucial parameter is the backaction damping (or optical damping) rate $\gamma_{\rm BA}$: this is the enhanced damping of the mechanical resonator resulting from a net energy loss to the driven cavity. The cooling power of the cavity backaction will be directly proportional to $\gamma_{\rm BA}$. In the low-frequency regime, a simple classical linear-response argument yields that, for a mechanical resonator dispersively coupled to a cavity, $\gamma_{\rm BA} \propto d\bar{n}/d\Delta$ [37,43]. As discussed in Ref. [8], thus, one expects that a nonlinear cavity will be capable of much stronger backaction damping than a linear cavity, given the enhanced slope of the cavity response curve (cf. Fig. 3).

A large backaction damping is not, however, in itself enough to ensure good cooling. One needs that the cavity acts as a source of *cold* damping for the mechanical resonator. Thus, one must also consider the effective temperature of the backaction noise $T_{\rm BA}$. Reference [8] examined this quantity numerically; in contrast, our approach allows us to obtain simple analytic expressions in the interesting regime where one is near the bifurcation point and the parametric gain $G[0] \gg 1$.

Our analysis is based on the unsymmetrized backaction noise spectral density, defined as

$$S_{FF}[\omega] \equiv \int_{-\infty}^{\infty} dt\, \langle \hat{F}(t)\hat{F}(0)\rangle. \tag{56}$$

The symmetrized noise considered in Secs. II– V is given by $\bar{S}_{FF}[\omega] = (S_{FF}[\omega] + S_{FF}[-\omega])/2$. The frequency asymmetry of $S_{FF}[\omega]$ describes the asymmetry between emission and absorption of energy by the cavity; a standard perturbative calculation shows that it directly determines the backaction damping of the mechanical resonator [5]:

$$\gamma_{\rm BA}[\omega] = \frac{1}{2m\hbar\omega_m}(S_{FF}[+\omega] - S_{FF}[-\omega]), \tag{57}$$

where m is the oscillator mass. Using the linearized-Langevin approach described in Secs. II– V, we find a particular simple form for $\gamma_{\rm BA}$ near the bifurcation, in the limit where ω_M/Ω_B remains constant as the parametric gain $G \to \infty$:

$$\gamma_{\rm BA} \sim \frac{1}{\sqrt{3}}\frac{A^2\bar{n}}{\hbar m\kappa^2}\frac{G[0]}{1+(\omega/\Omega_B)^2} \equiv \frac{1}{\sqrt{3}}\frac{A^2\bar{n}}{\hbar m\kappa^2}G[\omega]. \tag{58}$$

In the $\omega_M \to 0$ limit, this reproduces the classical expression $\gamma_{\rm BA} \propto d\bar{n}/d\Delta$, while for nonzero frequency, we see that the backaction damping decays rapidly on the scale of the parametric amplification bandwidth Ω_B. The full expression (valid even for small G) is given in the Appendix. It is instructive to compare this result for $\gamma_{\rm BA}$ against the corresponding expression for a linear cavity, in the relevant limit $\omega_M \ll \kappa$, and for an optimized detuning [36,37]. As expected, one finds that the nonlinear cavity's $\gamma_{\rm BA}$ is enhanced by a factor of the parametric gain $G[\omega]$.

As already discussed, we must also consider the effective temperature $T_{\rm BA}[\omega]$ of the backaction, a quantity that is, in general, frequency dependent and is defined as [5]

$$\exp\left[-\frac{\hbar\omega}{k_B T_{\rm BA}[\omega]}\right] \equiv \frac{S_{FF}[-\omega]}{S_{FF}[+\omega]}. \tag{59}$$

Using our linearized-Langevin approach, we find a particularly simple asymptotic expression for the Bose-Einstein factor $n_{\rm BA}$ associated with $T_{\rm BA}[\omega]$ in the large-G limit relevant near the bifurcation:

$$1 + 2n_{\rm BA}[\omega] \equiv \coth\left(\frac{\hbar\omega}{2k_B T_{\rm BA}[\omega]}\right) \sim \frac{1+3(\omega/\kappa)^2}{\sqrt{3}(\omega/\kappa)}. \tag{60}$$

The full expression for $n_{\rm BA}$ is given in the Appendix. The expression for $n_{\rm BA}[\omega]$ is remarkably similar to the corresponding expression for a linear cavity [36,37]. In particular, the relevant frequency scale is κ and *not* the much smaller scale set by

the parametric bandwidth Ω_B. Thus, one finds that, in the low-frequency limit $\omega_M \ll \kappa$,

$$T_{\mathrm{BA}}[0] \sim \frac{\kappa}{2\sqrt{3}}. \tag{61}$$

In contrast, in the low-frequency limit, the effective backaction temperature of an optimally driven linear cavity is $\kappa/2$.

Thus, the effective backaction temperature of our nonlinear cavity near the bifurcation only differs by a numerical prefactor from that of a linear cavity. For low frequencies, the final oscillator temperature T_{osc} is given by [37]

$$T_{\mathrm{osc}} = \frac{\gamma_0 T_0 + \gamma_{\mathrm{BA}} T_{\mathrm{BA}}}{\gamma_0 + \gamma_{\mathrm{BA}}}. \tag{62}$$

Here, γ_0 is the oscillator damping resulting from its intrinsic (i.e., nonbackaction) sources of dissipation, and T_0 is the temperature of this bath. Thus, we have established that, for a low-frequency mechanical resonator, the nonlinear cavity is a far better way to cool than the linear cavity. One has a much greater backaction damping rate as well as a slightly smaller effective backaction temperature.

VII. CONCLUSIONS

In this paper, we have given a theoretical treatment of the quantum measurement properties of a driven nonlinear cavity used as a linear detector or amplifier. By using the equivalence between this system near its bifurcation point and a degenerate parametric amplifier driven by a detuned pump, we were able to give a relatively simple description of the physics. We find that quantum-limited amplification is indeed possible, but only if one is able to make use of the large correlations between backaction and imprecision noises. Such correlations are ideally suited for position detection of a mechanical system far from resonance; however, they cannot be utilized in QND qubit detection, and, hence, one is far from reaching the relevant quantum limit on this task. We also examined the possibility of backaction cooling using this system, demonstrating that the nonlinearity is particularly useful in the case where one wants to cool a mechanical resonator whose frequency is $\omega_M \ll \kappa$.

ACKNOWLEDGMENTS

We thank K. Lehnert and R. Vijay for useful discussions. This work was supported by NSERC, FQRNT, and the Canadian Institute for Advanced Research.

APPENDIX

1. Mapping to the Detuned DPA

Using Eqs. (18) and (19), the equation of motion for the displaced cavity annihilation operator $\hat{d}$ takes the form

$$\dot{\hat{d}} = (-\kappa/2 + i\widetilde{\Delta})\hat{d} + \tilde{g}\hat{d}^\dagger - \sqrt{\kappa}\hat{\xi}(t). \tag{A1}$$

Introducing the canonical quadratures,

$$\begin{pmatrix} \hat{x} \\ \hat{p} \end{pmatrix} = \frac{1}{\sqrt{2}}\begin{bmatrix} 1 & 1 \\ -i & i \end{bmatrix}\begin{pmatrix} \hat{d} \\ \hat{d}^\dagger \end{pmatrix}, \tag{A2}$$

and defining $\hat{x}_{\mathrm{in}}, \hat{p}_{\mathrm{in}}$ to be the corresponding quadratures of the noise operator $\hat{\xi}$, the equations of motion take the form

$$\frac{d}{dt}\begin{pmatrix} \hat{x} \\ \hat{p} \end{pmatrix} = \mathbf{M}\begin{pmatrix} \hat{x} \\ \hat{p} \end{pmatrix} - \sqrt{\kappa}\begin{pmatrix} \hat{x}_{\mathrm{in}} \\ \hat{p}_{\mathrm{in}} \end{pmatrix}. \tag{A3}$$

Here, $\mathbf{M}$ is the matrix defined as

$$\mathbf{M} = \begin{bmatrix} \tilde{g} - \frac{\kappa}{2} & -\widetilde{\Delta} \\ \widetilde{\Delta} & -\left(\tilde{g} + \frac{\kappa}{2}\right) \end{bmatrix}. \tag{A4}$$

Equation (A3) can conveniently be solved by first diagonalizing $\mathbf{M}$. The only subtlety is that, due to the nonzero effective drive detuning $\widetilde{\Delta}$, $\mathbf{M}$ is non-Hermitian; as a result, its eigenvectors are not orthogonal to one another. Defining θ as per Eq. (25), we let

$$\mathbf{V} = \begin{bmatrix} \cos(\theta/2) & \sin(\theta/2) \\ \sin(\theta/2) & \cos(\theta/2) \end{bmatrix} \tag{A5}$$

denote the matrix whose columns are the eigenvectors of $\mathbf{M}$. One then has

$$\mathbf{M} = -\mathbf{V}\begin{bmatrix} (\chi_1[0])^{-1} & 0 \\ 0 & (\chi_2[0])^{-1} \end{bmatrix}\mathbf{V}^{-1}, \tag{A6}$$

where the eigenvalues of $\mathbf{M}$ are just the inverses of the susceptibilities $\chi_1[0], \chi_2[0]$ defined in Eq. (27).

The rotation defining the quadratures $\hat{X}$ and $\hat{P}$ introduced in Eq. (24a) can now be written as

$$\begin{pmatrix} \hat{X} \\ \hat{P} \end{pmatrix} \equiv \mathbf{T}\begin{pmatrix} \hat{x} \\ \hat{p} \end{pmatrix} = \begin{bmatrix} \cos(\theta/2) & \sin(\theta/2) \\ -\sin(\theta/2) & \cos(\theta/2) \end{bmatrix}\begin{pmatrix} \hat{x} \\ \hat{p} \end{pmatrix}. \tag{A7}$$

The form of $\mathbf{M}$ makes it clear that $\hat{X}$, as defined in Eq. (24a), is indeed the amplified eigenquadrature of the cavity: It corresponds to the first eigenvector and eigenvalue of $\mathbf{M}$. In contrast, the orthogonal quadrature $\hat{P}$ defined in Eq. (24b) *does not* correspond to an eigenvector of $\mathbf{M}$.

Finally, Fourier transforming the equations of motion Eq. (A7) using the convention,

$$\hat{A}[\omega] \equiv \int_{-\infty}^{\infty} dt\, \hat{A}(t) e^{-i\omega t}, \tag{A8}$$

and making the above rotation, we find

$$(i\omega\mathbf{1} + \mathbf{T}\mathbf{M}\mathbf{T}^{-1})\begin{pmatrix} \hat{X}[\omega] \\ \hat{P}[\omega] \end{pmatrix} = \sqrt{\kappa}\begin{pmatrix} \hat{X}_{\mathrm{in}}[\omega] \\ \hat{P}_{\mathrm{in}}[\omega] \end{pmatrix}, \tag{A9}$$

where the identity matrix is $\mathbf{1}_{\mathrm{ij}} = \delta_{\mathrm{ij}}$. Solving for $\hat{X}[\omega]$ and $\hat{P}[\omega]$ directly yields Eqs. (26).

2. Backaction force

Using the definition of the backaction force operator $\hat{F}$ given in Eq. (31) and solutions to the cavity equations of motion, Eqs. (26), we find

$$\hat{F}[\omega] = F_{\mathrm{x}}[\omega]\hat{X}_{\mathrm{in}}[\omega] + F_{\mathrm{p}}[\omega]\hat{P}_{\mathrm{in}}[\omega], \tag{A10}$$

where

$$F_{\mathrm{x}}[\omega] \equiv -A\sqrt{2\bar{n}\kappa}\sin\nu\,\chi_1[\omega], \tag{A11a}$$

$$F_{\mathrm{p}}[\omega] \equiv -A\sqrt{2\bar{n}\kappa}\{(\chi_2[\omega] - \chi_1[\omega])\sin\nu\tan\theta + \chi_2[\omega]\cos\nu\}, \tag{A11b}$$

and the angle ν is defined in Eq. (32).

The unsymmetrized force noise spectral density $S_{FF}[\omega]$ defined in Eq. (56) can be written in terms of $\hat{F}[\omega]$ as

$$2\pi\delta(\omega+\omega')S_{FF}[\omega] = \langle \hat{F}[\omega]\hat{F}[\omega']\rangle. \tag{A12}$$

Thus, we can use Eq. (A10) to calculate $S_{FF}[\omega]$ if we know the correlation functions of the input noise operators $\hat{X}_{\rm in}$, $\hat{P}_{\rm in}$. From standard input-output theory and our assumption that $\hat{\xi}(t)$ describes vacuum noise, one easily finds

$$\langle \hat{X}_{\rm in}[\omega]\hat{X}_{\rm in}[\omega']\rangle = \pi\delta(\omega+\omega'), \tag{A13a}$$

$$\langle \hat{P}_{\rm in}[\omega]\hat{P}_{\rm in}[\omega']\rangle = \pi\delta(\omega+\omega'), \tag{A13b}$$

$$\langle \hat{X}_{\rm in}[\omega]\hat{P}_{\rm in}[\omega']\rangle = i\pi\delta(\omega+\omega'). \tag{A13c}$$

Explicitly computing the symmetrized spectral density $\bar{S}_{FF}[\omega] = (S_{FF}[\omega] + S_{FF}[-\omega])/2$, we find

$$\bar{S}_{FF}[\omega] = 4A^2\bar{n}\kappa \times \left(\frac{\kappa^2 + 6\tilde{g}^2 + 4\omega^2 - 2\tilde{g}^2(\cos 2\theta + 4\sin\theta)}{(\kappa^2+4\omega^2)^2 - 8\tilde{g}^2\cos^2\theta(\kappa^2 - 4\omega^2 - 2\tilde{g}^2\cos^2\theta)}\right). \tag{A14}$$

We have used the value of the angle ν given in Eq. (32). We stress that this expression only involves our initial linearization of the dynamics and does involve any further assumption of being close to the bifurcation. In the limit where one approaches the bifurcation (i.e., $\kappa\chi_1[0] \to \infty, \theta \to \pi/6$), one obtains the asymptotic form given in Eq. (47).

One can use Eq. (A14) to verify that $\bar{S}_{FF}[0]$ is indeed related to the derivative of $\langle\hat{a}\rangle$ with respect to Δ as per Eqs. (49) and (50). This is easily done using $\langle\hat{a}\rangle = \sqrt{\bar{n}}e^{i\phi_a}$, where $\bar{n}$ is given by Eq. (17), and the phase ϕ_a is given by

$$\tan\phi_a = -\frac{\kappa}{2\Delta + 4\Lambda\bar{n}} \tag{A15}$$

(as follows from the classical equations of motion).

Finally, we note that the above results are easily generalized for finite temperature. The input noise correlators in Eqs. (A13) and $\bar{S}_{FF}[\omega]$ are simply multiplied by $(1+\bar{n}_{\rm th})$, where $\bar{n}_{\rm th}$ is a Bose-Einstein factor evaluated at the temperature of the incident thermal noise and the frequency of the cavity.

3. Imprecision noise

The intensity $\hat{I}[\omega]$ of the homodyne measurement is given by Eq. (35). Using the solutions to the equation of motion in Eq. (26), we obtain

$$\hat{I}[\omega] = I_{\rm x}[\omega]\hat{X}_{\rm in} + I_{\rm p}[\omega]\hat{P}_{\rm in}, \tag{A16}$$

where

$$I_{\rm x}[\omega] = \sqrt{\kappa}\cos\varphi_h(1-\kappa\chi_1[\omega]), \tag{A17a}$$

$$I_{\rm p}[\omega] = \sqrt{\kappa}[\sin\varphi_h(1-\kappa\chi_2[\omega]) - \kappa\cos\varphi_h\tan\theta(\chi_2[\omega]-\chi_1[\omega])]. \tag{A17b}$$

It is now a straightforward exercise to compute the spectral density $S_{II}[\omega]$ from Eqs. (A16) and (A13), in complete analogy to our calculation of $S_{FF}[\omega]$. One finds this output noise to be completely symmetric in frequency: $S_{II}[\omega] = S_{II}[-\omega]$, and, thus, $S_{II}[\omega] = \bar{S}_{II}[\omega]$. The imprecision noise spectral density $\bar{S}_{zz}[\omega]$ then follows using Eqs. (6) and (37).

4. Imprecision-backaction correlation

The symmetrized imprecision-backaction noise correlator $\bar{S}_{IF}[\omega]$ may be written

$$\bar{S}_{IF}[\omega] = \tfrac{1}{2}(S_{IF}[\omega] + S_{IF}[-\omega]^*), \tag{A18}$$

where the unsymmetrized correlator is given by

$$2\pi\delta(\omega+\omega')S_{IF}[\omega] = \langle\hat{I}[\omega]\hat{F}[\omega']\rangle. \tag{A19}$$

Thus, we may calculate $\bar{S}_{IF}[\omega]$ using Eqs. (A10), (A16), and (A13); dividing by $\chi_{IF}[\omega]$ as given in Eq. (37) then yields the desired correlator $\bar{S}_{zF}[\omega]$.

5. Cooling

Using Eqs. (A11), one finds that the full expression for the asymmetric-in-frequency part of $S_{FF}[\omega]$ is given by

$$\frac{S_{FF}[+\omega] - S_{FF}[-\omega]}{\omega} = \frac{64A^2\bar{n}\tilde{g}\kappa(\sin\theta - 1)}{(\kappa^2+4\omega^2)^2 - 8\tilde{g}^2\cos^2\theta(\kappa^2 - 4\omega^2 - 2\tilde{g}^2\cos^2\theta)}. \tag{A20}$$

This expression then directly gives the backaction damping via Eq. (57).

Combining the above expression with Eq. (A14) for $\bar{S}_{FF}[\omega]$, we can find a general expression for $n_{\rm BA}[\omega]$, the effective temperature of the backaction expressed as a number of quanta [cf. Eq.(60)]. We have

$$1 + 2n_{\rm BA}[\omega] = \frac{\kappa^2 + 6\tilde{g}^2 + 4\omega^2 - 2\tilde{g}^2(\cos 2\theta + 4\sin\theta)}{8\tilde{g}\omega(\sin\theta - 1)}. \tag{A21}$$

We stress that Eqs. (A20) and (A21) do not involve an assumption of being near the bifurcation.

6. Reverse gain

The forward gain in our system was defined in Eq. (4), which, upon Fourier transforming, takes the form

$$\hat{I}[\omega] = \chi_{IF}[\omega]\hat{z}[\omega]. \tag{A22}$$

We derived $\chi_{IF}[\omega]$ in the main text by accounting for the coupling to $\hat{z}$ in the cavity equations of motion, resulting in Eq. (37).

In general, an amplifier may also have a reverse gain $\chi_{FI}[\omega]$; this describes how signals coupled to the output operator $\hat{I}$ could affect the average value of the backaction force operator $\hat{F}$ [5]. In general, reverse gain is undesirable, as it implies that measuring the detector output (by coupling to it) can lead to enhanced backaction fluctuations. The forms

of the fundamental quantum noise inequality of Eq. (11) are also modified in the presence of reverse gain.

To show that the reverse gain of our cavity amplifier vanishes, we make use of the equation [5],

$$\chi_{IF}[\omega] - \chi_{FI}[\omega]^* = -(i/\hbar)(S_{IF}[\omega] - S_{IF}[-\omega]^*). \quad \text{(A23)}$$

Using the solution of the cavity equations of motion to calculate $S_{IF}[\omega]$ and using the expression for $\chi_{IF}[\omega]$ from Eq. (37), Eq. (A23) directly yields that there is no reverse gain at any frequency:

$$\chi_{FI}[\omega] = 0. \quad \text{(A24)}$$

[1] J. D. Teufel, T. Donner, M. A. Castellanos-Beltrana, J. W. Harlow, and K. W. Lehnert, Nat. Nanotechnol. **4**, 820 (2009).

[2] J. B. Hertzberg, T. Rocheleau, T. Ndukum, M. Savva, A. A. Clerk, and K. C. Schwab, Nat. Phys. **6**, 213 (2010).

[3] D. I. Schuster, A. Wallraff, A. Blais, L. Frunzio, R.-S. Huang, J. Majer, S. M. Girvin, and R. J. Schoelkopf, Phys. Rev. Lett. **94**, 123602 (2005).

[4] J. Majer *et al.*, Nature (London) **449**, 443 (2007).

[5] A. A. Clerk, M. H. Devoret, S. M. Girvin, F. Marquardt, and R. J. Schoelkopf, Rev. Mod. Phys. **82**, 1155 (2010).

[6] B. Yurke, J. Opt. Soc. Am. B **4**, 1551 (1987).

[7] B. Yurke, L. R. Corruccini, P. G. Kaminsky, L. W. Rupp, A. D. Smith, A. H. Silver, R. W. Simon, and E. A. Whittaker, Phys. Rev. A **39**, 2519 (1989).

[8] P. D. Nation, M. P. Blencowe, and E. Buks, Phys. Rev. B **78**, 104516 (2008).

[9] R. Movshovich, B. Yurke, P. G. Kaminsky, A. D. Smith, A. H. Silver, R. W. Simon, and M. V. Schneider, Phys. Rev. Lett. **65**, 1419 (1990).

[10] M. A. Castellanos-Beltran, K. D. Irwin, G. C. Hilton, L. R. Vale, and K. W. Lehnert, Nat. Phys. **4**, 929 (2008).

[11] T. Yamamoto, K. Inomata, M. Watanabe, K. Matsuba, T. Miyazaki, W. D. Oliver, Y. Nakamura, and J. S. Tsai, Appl. Phys. Lett. **93**, 042510 (2008).

[12] B. Yurke and E. Buks, J. Lightwave Technol. **24**, 5054 (2006).

[13] E. Babourina-Brooks, A. Doherty, and G. Milburn, New J. Phys. **10**, 105020 (2008).

[14] I. Siddiqi, R. Vijay, F. Pierre, C. M. Wilson, M. Metcalfe, C. Rigetti, L. Frunzio, and M. H. Devoret, Phys. Rev. Lett. **93**, 207002 (2004).

[15] A. Lupaşcu, E. F. C. Driessen, L. Roschier, C. J. P. M. Harmans, and J. E. Mooij, Phys. Rev. Lett. **96**, 127003 (2006).

[16] I. Serban, M. I. Dykman, and F. K. Wilhelm, Phys. Rev. A **81**, 022305 (2010).

[17] V. B. Braginsky and F. Y. Khalili, *Quantum Measurement* (Cambridge University Press, Cambridge, UK, 1992).

[18] M. Hartridge, R. Vijay, D. H. Slichter, J. Clarke, and I. Siddiqi, e-print arXiv:1003.2466 (2010).

[19] R. Vijay, D. H. Slichter, and I. Siddiqi, e-print arXiv:1009.2969 (2010).

[20] F. R. Ong, M. Boissonneault, F. Mallet, A. Palacios-Laloy, A. Dewes, A. C. Doherty, A. Blais, P. Bertet, D. Vion, and D. Esteve, e-print arXiv:1010.6248 (2010).

[21] H. J. Carmichael, G. J. Milburn, and D. F. Walls, J. Phys. A **17**, 469 (1984).

[22] M. I. Dykman, Sov. Phys. Solid State **20**, 1306 (1978).

[23] C. W. Gardiner and M. J. Collett, Phys. Rev. A **31**, 3761 (1985).

[24] C. W. Gardiner and P. Zoller, *Quantum Noise* (Springer, Berlin, 2000).

[25] H. A. Haus and J. A. Mullen, Phys. Rev. **128**, 2407 (1962).

[26] C. M. Caves, Phys. Rev. D **26**, 1817 (1982).

[27] M. H. Devoret and R. J. Schoelkopf, Nature (London) **406**, 1039 (2000).

[28] A. A. Clerk, S. M. Girvin, and A. D. Stone, Phys. Rev. B **67**, 165324 (2003).

[29] M. I. Dykman, D. G. Luchinsky, R. Mannella, P. V. E. McClintock, N. D. Stein, and N. G. Stocks, Phys. Rev. E **49**, 1198 (1994).

[30] A. Blais, R.-S. Huang, A. Wallraff, S. M. Girvin, and R. J. Schoelkopf, Phys. Rev. A **69**, 062320 (2004).

[31] J. Gambetta, A. Blais, D. I. Schuster, A. Wallraff, L. Frunzio, J. Majer, M. H. Devoret, S. M. Girvin, and R. J. Schoelkopf, Phys. Rev. A **74**, 042318 (2006).

[32] G. J. Milburn and D. F. Walls, Opt. Commun. **39**, 401 (1981).

[33] T. Corbitt and N. Mavalvala, J. Opt. B **6**, S675 (2004).

[34] A. Buonanno and Y. Chen, Phys. Rev. D **64**, 042006 (2001).

[35] F. Marquardt and S. M. Girvin, Phys. **2**, 40 (2009).

[36] I. Wilson-Rae, N. Nooshi, W. Zwerger, and T. J. Kippenberg, Phys. Rev. Lett. **99**, 093901 (2007).

[37] F. Marquardt, J. P. Chen, A. A. Clerk, and S. M. Girvin, Phys. Rev. Lett. **99**, 093902 (2007).

[38] J. D. Teufel, J. W. Harlow, C. A. Regal, and K. W. Lehnert, Phys. Rev. Lett. **101**, 197203 (2008).

[39] T. Rocheleau, T. Ndukum, C. Macklin, J. B. Hertzberg, A. Clerk, and K. Schwab, Nature (London) **463**, 72 (2010).

[40] S. Groblacher, J. B. Hertzberg, M. R. Vanner, G. D. Cole, S. Gigan, K. C. Schwab, and M. Aspelmeyer, Nat. Phys. **5**, 485 (2009).

[41] Y.-S. Park and H. Wang, Nat. Phys. **5**, 489 (2009).

[42] A. Schliesser, O. Arcizet, R. Riviere, G. Anetsberger, and T. J. Kippenberg, Nat. Phys. **5**, 509 (2009).

[43] C. Höhberger-Metzger and K. Karrai, Nature (London) **432**, 1002 (2004).